Proceedings of the Thirty-fifth (2025) International Ocean and Polar Engineering Conference **www.isope.org**
Seoul/Goyang, Korea, June 1-6, 2025

ISBN 978-1-880653-74-6; ISSN 1098-6189

Finite-element model for geometric nonlinearity and dynamic stiffness of synthetic mooring lines

Shagun Agarwal and Oriol Colomés
Faculty of Civil Engineering and Geosciences, Delft University of Technology, Delft, The Netherlands

ABSTRACT

Synthetic mooring lines are increasingly considered for lightweight offshore renewables, but their elasticity poses modelling challenges due to large deformations and frequency-dependent dynamic and non-linear stiffness. To address this, we developed a finite element model based on finite-strain theory and dynamic stiffness. We utilise Tangential Differential Calculus for large deformation analysis and Schapery viscoelastic model for the non-linear constitutive relationship. Our results show that in taut systems, viscoelastic effects dominate at higher frequencies, leading to creep and relaxation under cyclic loads. In catenary systems without a chain segment, viscoelastic impacts are minimal due to low tension in the synthetic line.

KEY WORDS: Mooring; TDC; Viscoelasticity; Nonlinear constitutive model; Schapery; FEM.

INTRODUCTION

As demand grows for offshore floating structures, such as floating wind, floating solar, and wave-energy converters, the need for efficient, adaptable mooring systems has risen. Conventional chain-based mooring lines often prove costly, heavy, and overbuilt for these lightweight applications. Lighter mooring systems made with synthetic lines often a cost-competitive and lightweight option for such systems. However, their restoring mechanism relies on the elasticity of the line. This presents two unique challenges in their modelling; 1) the large deformation of the line, introducing geometric nonlinearity, and 2) their dynamic stiffness, where the stiffness if the line depends on the amplitude and frequency of the motion, along with the preceding history of the response. Therefore, there is a gap in the understanding of the deployment and operation of synthetic mooring lines in offshore systems

The Schapery non-linear viscoelastic model (Schapery, 1969) is a well-established framework for capturing the complex behaviour of viscoelastic materials, including fibre-reinforced polymers and biological tissues (Jamshidi and Shokrieh, 2024; Banks et al., 2011). However, its application to synthetic mooring lines remains relatively unexplored. Contemporary open-source mooring software, such as MoorDyn (Hall and Goupee, 2015), allows for the prescription of load-dependent stiffness but does not fully incorporate key viscoelastic characteristics such as retardation, creep, and stress relaxation. These properties can significantly influence mooring line response and loading conditions (Weller et al., 2015). Addressing this gap, recent work by Nguyen and Thiagarajan (2022) introduced SYNCOM, a constitutive modelling tool designed to integrate the viscoelastic properties of synthetic mooring lines into open-source mooring analysis frameworks like MoorDyn. However, this approach has a few potential limitations: 1) MoorDyn employs a lumped mass and explicit formulation, which may introduce stability and accuracy constraints, and 2) it follows a partitioned approach, where the constitutive relationship is solved separately from the mooring analysis, necessitating the use of an explicit formulation.

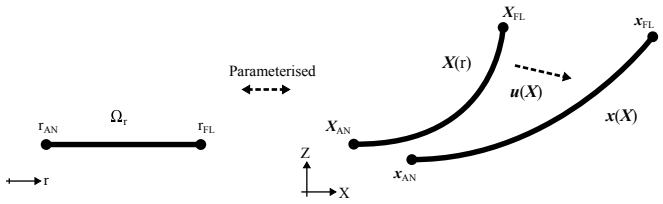

Fig. 1 Schematic for reference, undeformed and deformed configurations of a flexible cable.

In this manuscript, we present a unified finite-element model that implicitly integrates flexible mooring lines governed by finite-strain theory and non-linear viscoelastic material behaviour. We use the Tangential Differential Calculus (TDC) approach (Fries and Schöllhammer, 2020) for defining the continuous geometric and differential quantities associated with large deformation analysis of mooring lines on curved manifolds. The dynamic stiffness of the line is defined using a non-linear Schapery viscoelastic model, where the viscoelastic strain is a non-linear function of the stress at each time-step, including an instantaneous compliance and a transient compliance component. The coefficients of the viscoelastic model are based on real-scale laboratory experiments on synthetic lines. A key feature of the model is the ability to track the hereditary state of each quadrature point along the line, thereby allowing

compliance history to be independently monitored throughout the line.

The manuscript first briefly presents the formulation of the finite-element model for finite-strain theory, followed by a concise explanation of the non-linear and dynamic stiffness model. The FE model is then used to investigate the impact of the dynamic stiffness on the stress and strain at the fairlead for a taut and catenary mooring line, subjected to sinusoidal motion at the fairlead.

GOVERNING EQUATIONS

The modelling of flexible mooring lines involves three sources of non-linearities, 1) geometric nonlinearity from finite-strain or large displacement of the flexible cable; 2) dynamic and non-linear stiffness arising from the constitutive relationship for the mooring line material; 3) the behaviour of the sea-bed. We briefly describe the numerical model for each of these components.

Geometric Nonlinearity

We restrict our analysis to cables in 2D space $\mathbb{R}^2$. In finite-strain theory, the initial un-deformed manifold Γ_X and the dynamic deformed manifold Γ_x are denoted by $\boldsymbol{X}(r)$ and $\boldsymbol{x}(X)$. The difference between the two is the dynamic displacement field $\boldsymbol{u}(\boldsymbol{X}, t)$,

$$\boldsymbol{x}(\boldsymbol{X}, t) = \boldsymbol{X}(r) + \boldsymbol{u}(\boldsymbol{X}, t) \quad \text{where } \boldsymbol{X} \in \Gamma_X \subset \mathbb{R}^2 \text{ and } \boldsymbol{x} \in \Gamma_x \subset \mathbb{R}^2 \tag{1}$$

These manifolds are parametrised to 1D reference domain, $\Omega_r \subset \mathbb{R}^1$, with r representing the parametric coordinate on the line. Fig. 1 presents a schematic of these configurations.
The differential and geometric quantities from Tangential Differential Calculus (TDC) are used for defining the strain in the line. The directional and tangential Cauchy-Green strain tensors are defined on Γ_X as

$$\mathbf{E}_{\text{dir}} = \frac{1}{2} \cdot \left(\mathbf{F}_\Gamma^T \cdot \mathbf{F}_\Gamma - \mathbf{I} \right), \tag{2}$$

$$\mathbf{E}_{\text{tang}} = \mathbf{P} \cdot \mathbf{E}_{\text{dir}} \cdot \mathbf{P}. \tag{3}$$

Here $\mathbf{F}_\Gamma$ is the surface deformation gradient.
In this manuscript we will consider non-linear viscoelastic material. The constitutive relationship will be defined between the second Piola-Kirchhoff stress tensor $\mathbf{S}$ and the tangential Cauchy-Green strain tensors $\mathbf{E}_{\text{tang}}$, both defined on Γ_X. Once $\mathbf{S}$ is known, the first Piola-Kirchhoff stress tensors $\mathbf{K}$ on Γ_X and the Cauchy stress tensor $\boldsymbol{\sigma}$ on Γ_x are expressed as follows,

$$\mathbf{K} = \mathbf{F}_\Gamma \cdot \mathbf{S}, \tag{4}$$

$$\boldsymbol{\sigma} = \frac{1}{\Lambda} \cdot \mathbf{F}_\Gamma \cdot \mathbf{S} \cdot \mathbf{F}_\Gamma, \tag{5}$$

where Λ is the local measure of elongation.

Fig. 2 presents the schematic of the mooring line problem studied in this manuscript. In our analysis, a cable with initial length L_0 is bounded by the anchor $\boldsymbol{X}_{\text{AN}} = \boldsymbol{X}(r = 0)$ and the fairlead $\boldsymbol{X}_{\text{FL}} = \boldsymbol{X}(r = L_0)$. The forces on the line considered in this analysis include the action of gravity $\boldsymbol{b}_{\text{weight}}$, the buoyancy due to the surrounding fluid $\boldsymbol{b}_{\text{buoyancy}}$ and the reaction from the sea-bed $\boldsymbol{b}_{\text{bed}}$, which is modelled using a damped spring bed formulation.

$$\boldsymbol{b}_{\text{bed}}(\boldsymbol{x}) = \begin{cases} -k_b \left(z - z_{\text{bed}} \right) \hat{k} - c_b \dot{z} \hat{k} & \text{if } z \le z_{\text{bed}} \\ 0 & \text{if } z > z_{\text{bed}} \end{cases} \tag{6}$$

Here k_b and c_b are the spring constant and damping constant for the bed. Since the primary focus of this study is to examine the effects of viscoelastic material, the influence of drag has not been included in the

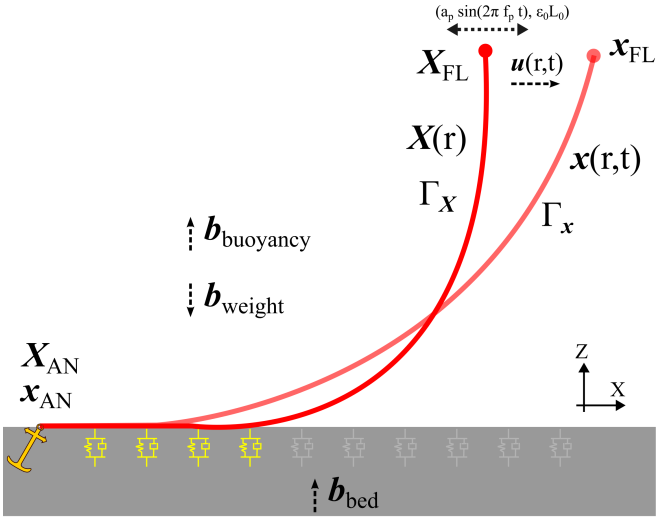

Fig. 2 Schematic for the mooring line

analysis. The equilibrium is defined on Γ_x as,

$$\rho \ddot{\boldsymbol{u}} - \text{div}_\Gamma \boldsymbol{\sigma}(\boldsymbol{u}) - \boldsymbol{b}(\boldsymbol{x}) = 0 \quad \forall \boldsymbol{x} \in \Gamma_x. \tag{7}$$

Here, ρ is density of the line, and $\boldsymbol{b}(\boldsymbol{x})$ is the vector sum of all forces. Since the deformed configuration is not known a priori, the finite-element problem is formulation on the undeformed configuration Γ_X by using the TDC based geometric quantities as defined earlier.
Consider the test function $\boldsymbol{w}$ and the trial function for displacement field $\boldsymbol{u}$ in a $[H^1(\Gamma_X)]^2$ function space. The weak form of the problem in the reference domain Γ_X is defined as

$$\begin{aligned} A \int_{\Omega_r} \rho_0 \, \boldsymbol{w} \cdot \ddot{\boldsymbol{u}} \, \|\mathbf{J}\| \, d\Omega + A \int_{\Omega_r} \left(\nabla_r \boldsymbol{w} \cdot \mathbf{Q}^T \right) : \mathbf{K}(\boldsymbol{u}) \, \|\mathbf{J}\| \, d\Omega \\ - A \int_{\Omega_r} \boldsymbol{w} \cdot \boldsymbol{B} \, \|\mathbf{J}\| \, d\Omega - \int_{\partial\Omega_r} \boldsymbol{w} \cdot \mathbf{H} \, d\partial\Omega = 0 \end{aligned} \tag{8}$$

Here, $\boldsymbol{B}$ represents the vector sum of the previously mentioned weight, buoyancy, and bed forces acting on the line, transformed into the reference configuration Γ_X. The term $\mathbf{H}$ denotes the boundary tension, which arises from integration by parts and can be utilized to apply boundary conditions through boundary tension. For brevity, we refer the readers to Fries and Schöllhammer (2020) for the definitions of the manifold Jacobian $\mathbf{J}$, geometric quantities $\mathbf{Q}$ and surface deformation gradient $\mathbf{F}_\Gamma$.
In this study, the boundary conditions on the line are enforced using the displacement field. The anchor is fixed with $\boldsymbol{u}_{\text{AN}} = [0, 0]^T$, while the fairlead undergoes a prescribed motion given by $\boldsymbol{u}_{\text{FL}} = [a_p \sin(2\pi f_p), \, \epsilon_0 L_0]^T$. Alternatively, the boundary conditions can also be imposed using boundary tension via $\mathbf{H}$.

Dynamic non-linear stiffness

We model the viscoelastic behaviour of synthetic mooring lines using the Schapery non-linear viscoelastic model (Schapery, 1969).
The constitutive relationship in for one dimensional case is expressed as

$$\varepsilon_{ve} = g_0 D_0 \sigma(t) + g_1 \int_0^t \Delta D \left(\psi(t) - \psi(\tau) \right) \frac{d(g_2 \sigma)}{dt} \, d\tau \tag{9}$$

Here the viscoelastic strain ε_{ve} is expression in terms of the instantaneous compliance D_0, transient compliance ΔD and load-rate response. Furthermore, the functions $g_0(\sigma)$, $g_1(\sigma)$ and $g_2(\sigma)$ represent the non-linearity in the instantaneous, transient and load-rate response. The ef-

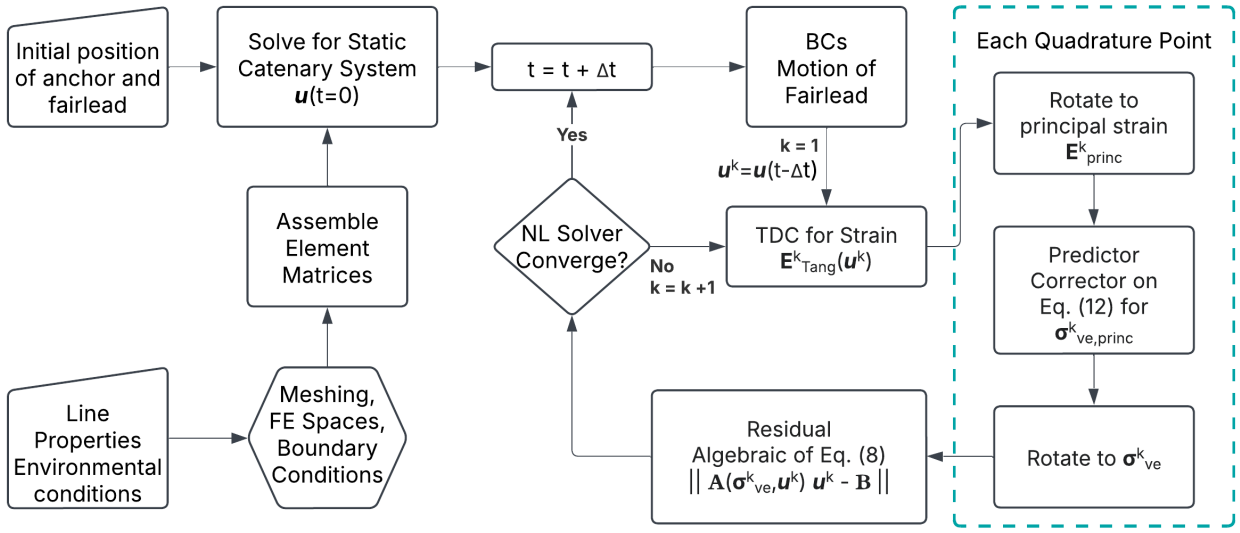

Fig. 3 Flowchart briefly illustrating the implementation of the geometrically non-linear system with a viscoelastic constitutive relationship.

Table 1 Viscoelastic parameters employed in quasi-static test for Rope 1.

Viscoelastic Parameter		
n	λ_n (s^{-1})	D_n (10^{-10} **Pa**$^{-1}$)
1	10^{-1}	1.0
2	10^{-2}	1.5
3	10^{-3}	1.0
4	10^{-4}	1.5
5	10^{-5}	20.0
6	10^{-6}	1.0
7	10^{-7}	1.0
8	10^{-8}	100.0
D_0	1.0835×10^{-10} Pa^{-1}	
$g_0 = 1.0 - 1.82e\text{-}10\ \sigma - 5.45e\text{-}18\ \sigma^2 + 1.82e\text{-}26\ \sigma^3$		
$g_1 = 0.1 + 6.6e\text{-}11\ \sigma + 4.2e\text{-}19\ \sigma^2 - 2.7e\text{-}27\ \sigma^3$		
$g_2 = 1.7 - 8.8e\text{-}9\ \sigma + 4.4e\text{-}17\ \sigma^2 + 5.0e\text{-}28\ \sigma^3$		

fective time ψ is given by

$$\psi = \int_0^t \frac{ds}{a_T a_\sigma a_e} \tag{10}$$

where a_T, a_σ and a_e represent the temperature, stress and environmental scaling factors. In this study we set each of these to unity.
The uniaxial transient compliance is expressed using a Prony series

$$\Delta D(\psi) = \sum_{n=1}^{N} D_n \left[1 - e^{-\lambda_n \psi}\right] \tag{11}$$

where λ_n is the retardation time and D_n is the corresponding compliance and N is the number of Prony series terms

Conducting experiments under tension (stress) control is generally easier than under strain control. Therefore, the compliance-based constitutive relation in Eq. 9, where viscoelastic strain is expressed as a function of stress and stress rate, is preferred for experimental analysis. However, the finite-element model used in this study is displacement-based, meaning that displacement and strain are prescribed, while the corresponding stress is unknown. To address this, the predictor-corrector incremental strain approach from Haj-Ali and Muliana (2004) is employed to integrate the Schapery non-linear viscoelastic model within the displacement-based finite-element framework.
Briefly, the incremental strain approach computes the strain at the current time step, ε^t , given the strain from the previous time step. The uniaxial stress σ^t corresponding to the strain ε^t is given by

$$\begin{aligned}\Delta\varepsilon^t = \varepsilon^t - \varepsilon^{t-\Delta t} = \\ \bar{D}^t\sigma^t - \bar{D}^{t-\Delta t}\sigma^{t-\Delta t} - \sum_{n=1}^{N} D_n \left(g_1^t\ \exp(\lambda_n \Delta\psi^t) - g_1^{t-\Delta t}\right) q_n^{t-\Delta t} \\ - g_2^{t-\Delta t} \sum_{n=1}^{N} D_n \left[\begin{array}{l} g_1^{t-\Delta t}\left(\dfrac{1-\exp(\lambda_n\Delta\psi^{t-\Delta t})}{\lambda_n\Delta\psi^{t-\Delta t}}\right) \\ \qquad - g_1^t\left(\dfrac{1-\exp(\lambda_n\Delta\psi^t)}{\lambda_n\Delta\psi^t}\right)\end{array}\right]\sigma^{t-\Delta t}\end{aligned} \tag{12}$$

Here, $\bar{D}$ is the effective instantaneous dynamic compliance and q_n^t is the heredity integral for the n^{th} Prony series component. We refer the readers to Haj-Ali and Muliana (2004) for the expressions for these terms.
The above equation is implicit in σ^t and is therefore solved using the predictor-corrector fixed-point iteration method, starting with an initial guess of $\sigma^t = \sigma^{t-\Delta t}$. In this analysis, the uniaxial viscoelastic constitutive relationship is applied to the principal $\mathbf{E}_{\text{tang}}$ strains and the corresponding principal **S** stresses. At each quadrature point, the procedure involves first computing the $\mathbf{E}_{\text{tang}}$ tensor, rotating it to obtain the principal strains, applying the constitutive relationship to determine the corresponding viscoelastic principal **S** stresses, and finally rotating back to reconstruct the **S** tensor. This process is repeated at each quadrature point, after which the residual of the weak form is assembled to construct the system of equations.
The weak form Eq. 8 is solved on a discretized reference domain, Ω_r, which is represented using line elements with quadratic polynomial test and trial functions. The resulting system is then solved using a Newton-Raphson solver. The time-stepping for the second order ordinary differential equation is done using the Generalised-α method (Chung and Hulbert, 1993), with the parameter $\rho_\infty = 0$ for dissipation of frequencies higher $f > 10/\Delta t$. The finite element model is developed in Julia using

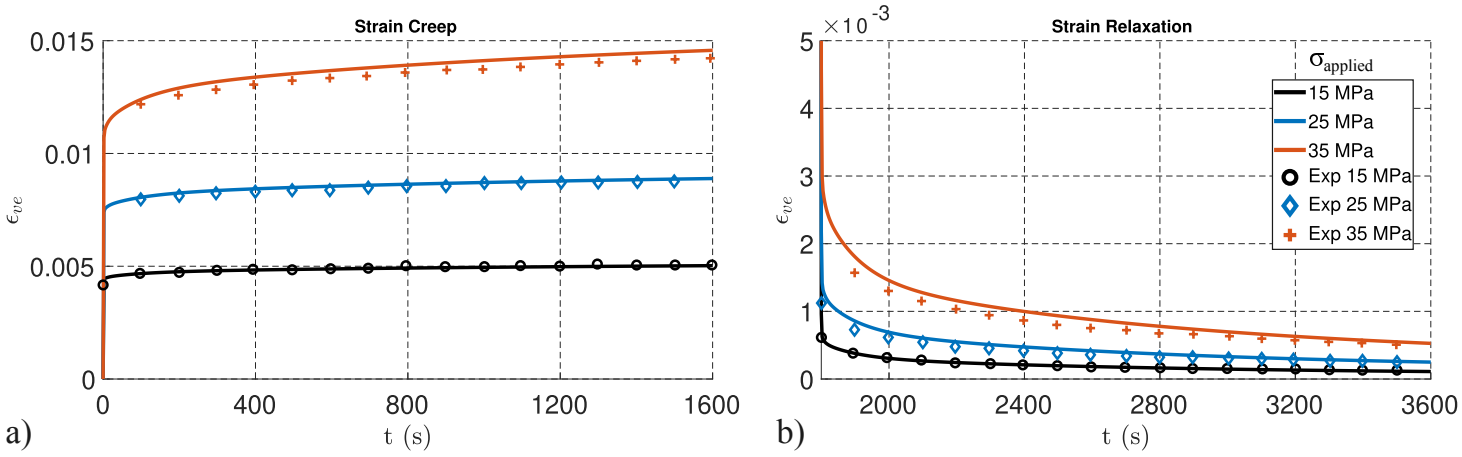

Fig. 4 Time-series of viscoelastic strain ε_{ve} obtained from the numerical model, compared against experiments from Lai and Bakker (1996) for creep-relaxation tests for stresses {15, 25, 35} MPa. a) Creep stage. b) Relaxation stage.

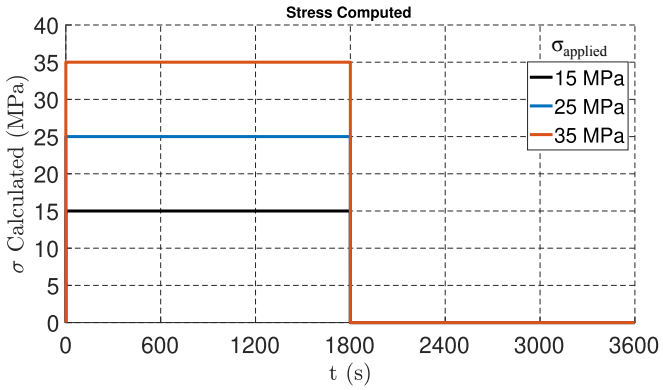

Fig. 5 Time series of stress σ calculated using predictor-corrector approach applied to Eq. 12.

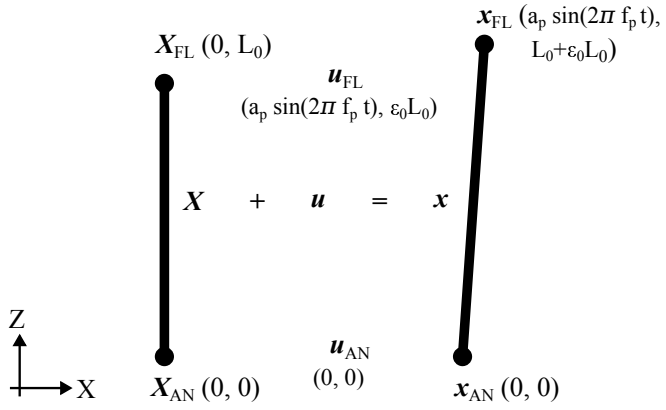

Fig. 6 Schematic for taut line setup

the open-source library *Gridap.jl* (Badia and Verdugo, 2020). A brief overview of this solution algorithm is illustrated in Fig. 3.

RESULTS AND DISCUSSION

The numerical tests are conducted on the Kapa Polyester Plus rope, which has a diameter of 52 mm and a Minimum Breaking Force (MBF) of 1.021 MN. The experimental investigation of this rope, along with its material characterization, is detailed in Colomés et al. (2025). In Colomés et al. (2025), the parameters of the non-linear Schapery viscoelastic model were determined through a systematic approach. They conducted uniaxial excitation experiments on a segment of the mooring line, where the applied tension was controlled, and the resulting strain was measured. These tests covered a range of loading conditions, including creep-relaxation loading and cyclic loading at different amplitudes, frequencies, and mean stress levels. They employed the *Particle Swarm Optimization* technique to determine the values of the transient compliance coefficients D_n and the polynomial coefficients for g_0, g_1, and g_2. The final characterization of the rope is summarized in Table 1.

We study the behaviour of this line, when used in a taut mooring system or a catenary mooring system. Moreover, we also investigate the difference in response, considering three different constitutive relationships,

1. Linear Elastic (LE): The linear compliance is taken as D_0 from Table 1.
2. Linear Viscoelastic (LVE): The transient compliance D_n values from Table 1 are considered. However, the model is linearized by setting the functions to fixed values: $g_0 = 1.0$, $g_1 = 0.1$, and $g_2 = 1.7$, thereby eliminating their dependence on stress.
3. Non-linear viscoelastic (NLVE): Considering the complete parametrisation in Table 1.

The comparison between NLVE and LVE will provide insights into the extent to which compliance nonlinearity influences the system's response.

Verification via stress-relaxation test

The numerical model presented in this manuscript is validated against creep-relaxation tests reported in Lai and Bakker (1996), which were conducted on the glassy amorphous polymer PMMA. The viscoelastic properties used in our analysis are taken from Table 1 in Nguyen and Thiagarajan (2022). In the test, a constant stress of $\sigma_{applied}$ is applied to the cable, and the strain is recorded over 1800s to capture the strain creep phase. The stress is then reduced to 0 MPa, and the viscoelastic strain is monitored to observe the strain relaxation phase.

$$\sigma(t) = \begin{cases} \sigma_{applied}, & 0 < t < 1800 \\ 0, & t = 0 \text{ and } t \geq 1800 \end{cases} \tag{13}$$

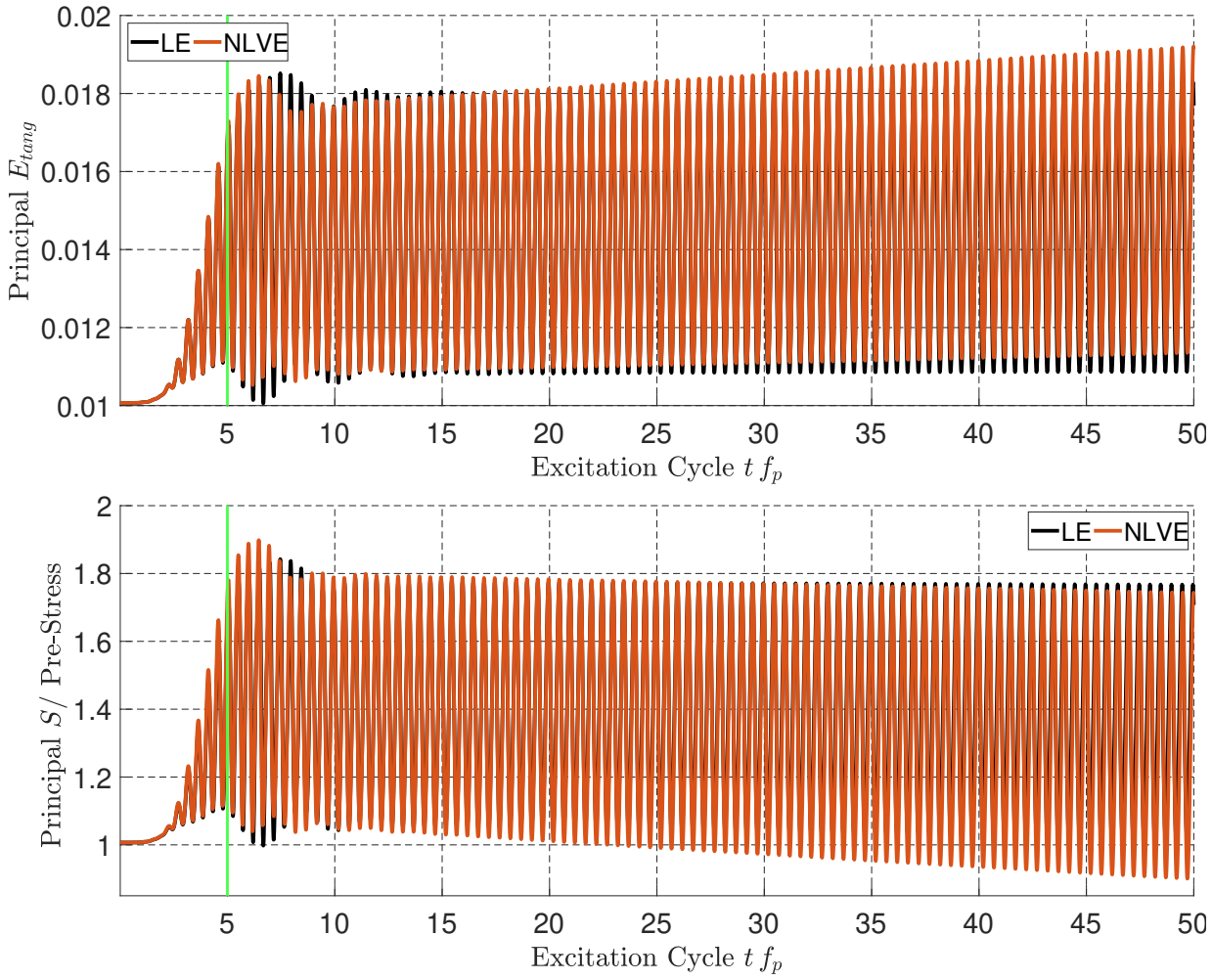

Fig. 7 Plots of principal strain $\mathbf{E}_{\text{tang}}$ and principal stress $\mathbf{S}$ at the fairlead, for taut mooring line subjected to $f_p = 3.05\,\text{Hz}$ and $a_p = 2.0\,\text{m}$. The results are compared across linear-elastic (LE) and non-linear viscoelastic (NLVE) constitutive relationships.

We study the cases $\sigma_{\text{applied}} \in \{15, 25, 35\}\,\text{MPa}$. Figure 4a,b compares the viscoelastic strain predicted by the numerical model with the experimental data from Lai and Bakker (1996) during the creep and relaxation stages, respectively.

To verify the implementation of the predictor-corrector algorithm used for Eq. 12, the applied stress is recalculated from the strain time series shown in Fig. 4. The resulting stress time series is presented in Fig. 5, where it closely matches the applied stress with an error of less than $10^{-7}\,\text{MPa}$, confirming the accuracy of the numerical implementation.

Taut Line

We now conduct a study on periodic transverse excitation of a taut mooring line, with the problem schematic shown in Fig. 6. The line has un-deformed length $L_0 = 100\,\text{m}$, dry density $\rho_0 = 1380\,\text{kg m}^{-3}$, area of cross-section $A = 0.00212371663\,\text{m}^2$, initial axial stretch $\epsilon_0 = 0.01$, resulting in a pre-tension of 196 kN. The taut line is fixed at the anchor $\boldsymbol{x}_{AN}$, while the $\boldsymbol{x}_{FL}$ fairlead undergoes sinusoidal horizontal motion with excitation frequency f_p and amplitude a_p. For these conditions, the first three linear natural frequencies of the taut string are $f_{1,2,3} = 1.29, 2.59, 3.88\,\text{Hz}$, based on the expression $f_n = \frac{n}{2L_0}\sqrt{\frac{E\epsilon_0}{\rho_0}}$ Consequently, we study the taut line in the vicinity of these linear natural frequencies.

We begin by analyzing the case with $f_p = 3.05\,\text{Hz}$ and $a_p = 2.0\,\text{m}$. In each test case, the excitation amplitude at the fairlead is gradually increased over five cycles before reaching the prescribed amplitude, ensuring a smooth transition and minimizing the effects of a sudden start. The simulations are then run for 50 cycles to highlight the viscoelastic effects. Fig. 7 presents the time-series for the principal strain $\mathbf{E}_{\text{tang}}$ and principal stress $\mathbf{S}$ at the fairlead over 50 cycles, comparing results obtained from both LE and NLVE constitutive models. Once the transient effects from the ramp-up phase diminish, the LE simulation reaches a steady state. In contrast, the NLVE time-series exhibits an increasing mean strain value due to creep, along with a gradual relaxation of the mean stress over time. In order to better understand the stiffness of the line, we plot the principal strain $\mathbf{E}_{\text{tang}}$ against the principal stress $\mathbf{S}$ for the final 25 excitation cycles in Fig. 8a. Here we also include the results from the LVE constitutive relationship, for highlighting the impact of the nonlinearity in the transient compliance. The LE result has a constant slope. When looking at the NLVE result, the plot is shifted to the right, implying higher strain, and towards the bottom, indicating lower stress. Infact, the plot "drifts" to bottom right in each successive excitation cycle. This is resultant from the viscoelasticity of the material. When looking at the LVE results, the drift is less predominant. Additionally, the NLVE response

exhibits a higher slope than the LVE response at high stress levels and a lower slope at low stress levels, highlighting the non-linear stiffness behaviour.
Finally, a zoomed-in view of the response during the final two excitation cycles is presented in Fig. 9a-b, comparing the results of LE, LVE and NLVE. This highlights that the LVE and NLVE responses exhibit significant phase difference relative to the LE response as a result of the damping introduced by the material viscoelasticity.

To gain a preliminary understanding of the impact of excitation frequency, we now examine a case where the excitation frequency is below the first linear natural frequency of the line. Specifically, we repeat the test for $f_p = 0.90\,\text{Hz}$ and $a_p = 2.0\,\text{m}$. The time-series of the principal strain $\mathbf{E}_{\text{tang}}$ and stress $\mathbf{S}$ at the fairlead for the final two excitation cycles is shown in Fig. 9c-d. Here, the impact of viscoelasticity on $\mathbf{E}_{\text{tang}}$ is minimal after 50 cycles, whereas some evidence of stress relaxation is observed. This trend is also reflected in the stiffness plot for this case, shown in Fig. 8b, which primarily drifts downward due to stress relaxation. These observations suggest that viscoelastic effects are more pronounced at higher excitation frequencies. When comparing NLVE and LVE results in Fig. 8b, a non-linear stiffness response is still observed, characterized by increased stiffness at higher stress levels.
Finally, we do an indicative study to examine the impact of excitation amplitude, by excitation the fairlead with $f_p = 3.05\,\text{Hz}, a_p = 1.0\,\text{m}$. The time-series of strain $\mathbf{E}_{\text{tang}}$ and stress $\mathbf{S}$ at the final two cycles are shown in Figs. 9e-f, while the stress-strain relationship is illustrated in Fig. 8c. From these figures, we observe strong stress relaxation and a pronounced phase lag, with minimal strain creep.

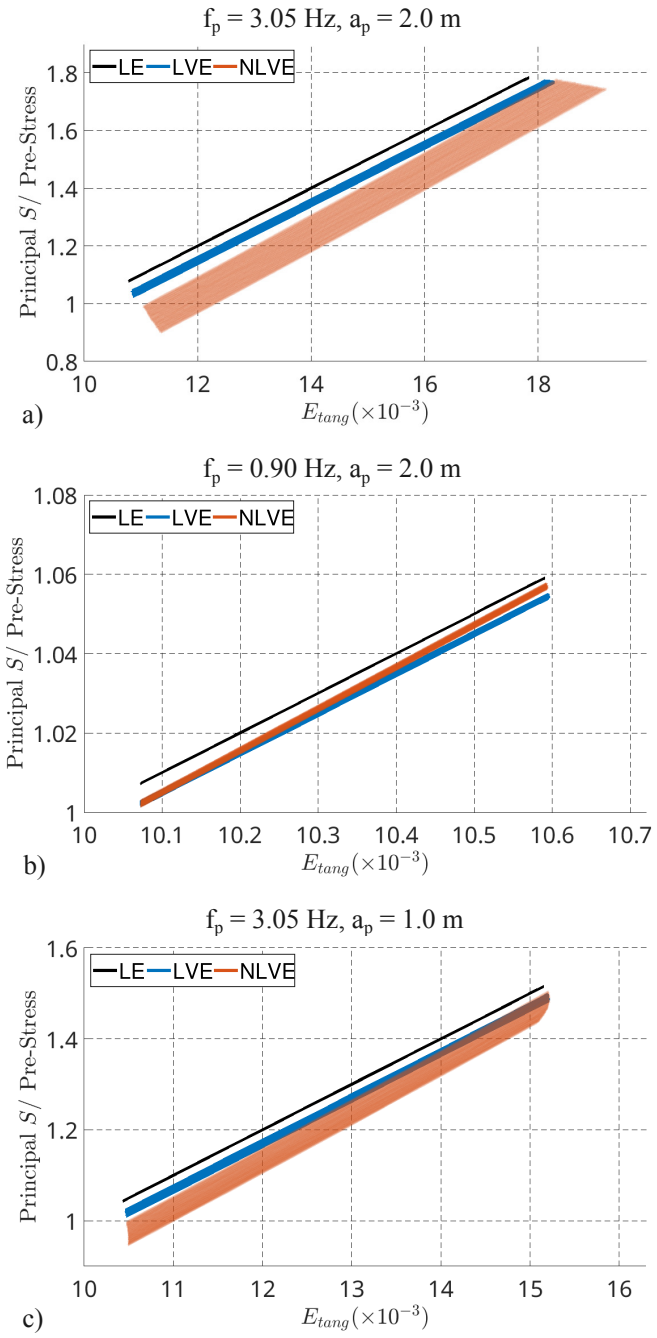

Fig. 8 Plots of principal $\mathbf{E}_{\text{tang}}$ strain against principal $\mathbf{S}$ stress at the fairlead, to indicate the stiffness of the line at the fairlead for the final 25 excitation cycles.

From these observations, we can draw two indicative conclusions. In general, the geometric nonlinearity in the response is expected to increase with increasing excitation frequency f_p and amplitude a_p. The observed creeping behaviour in strain appears to be associated with the presence of geometric nonlinearity since, in the cases presented in this study, strain creep is only evident in the high-frequency, high-amplitude scenario. Additionally, stress relaxation is primarily influenced by the material's viscoelasticity, with higher stress relaxation occurring at higher excitation frequencies. To substantiate these findings, we will conduct further tests and present a more detailed analysis in our future work.

Catenary Line

We consider a catenary line of un-deformed length $L_0 = 835.35\,\text{m}$, dry-density $\rho_0 = 1380\,\text{kg m}^{-3}$ and area of cross-section $A = 0.00212371663\,\text{m}^2$. The line is placed in water-depth of $h_0 = 186\,\text{m}$, with the anchor fixed at $\boldsymbol{x}_{AN} = [0.0, 0.0]^T\,\text{m}$ and the fairlead initially at $\boldsymbol{x}_{FL} = [796.73, 186.0]^T\,\text{m}$. We include the impact of weight and buoyancy, and ignore the impact of self-drag for this analysis. The sea-bed is modelled as a damped spring bed with stiffness $3 \times 10^6\,\text{Pa m}^{-1}$ and damping $3 \times 10^5\,\text{Pa s m}^{-1}$. A schematic of the line is shown in Fig. 2.
These line properties are similar to those of the chain line examined in Hall and Goupee (2015), with the key difference that the present study assumes the line is entirely composed of synthetic rope. In practice, mooring systems typically consist of multiple segments, with a chain at the seabed and synthetic rope near the floater to prevent rope damage. However, for this study, a hypothetical scenario is considered in which the entire line is made of synthetic rope.

The fairlead is subjected to forced sinusoidal surge excitation, with the excitation period 20 s and amplitude $a_p = 5.0\,\text{m}$.. This is one of the design cases reported in Haj-Ali and Muliana (2004). The time-series plots of the principal $\mathbf{E}_{\text{tang}}$ strain and principal $\mathbf{S}$ stress at the fairlead are shown in Fig. 10. Since in this case, the line is not exposed to a pre-stress, we non-dimensionalise the dynamic stress against the stress at the fairlead in static conditions.In the strain and stress time-series, we observe a very minimal impact of viscoelasticity in the response.
Fig. 11 presents the stress-strain relationship for the final 25 excitation cycles, highlighting the hysteresis in the viscoelastic response. However, the response exhibits minimal drift, and when comparing the LVE and NLVE results, the impact of nonlinearity also appears to be limited. This is primarily due to the specific catenary setup considered in our study, where the response is dominated by the restoring force from the weight of the line. For catenary line, the elasticity of the line material plays a

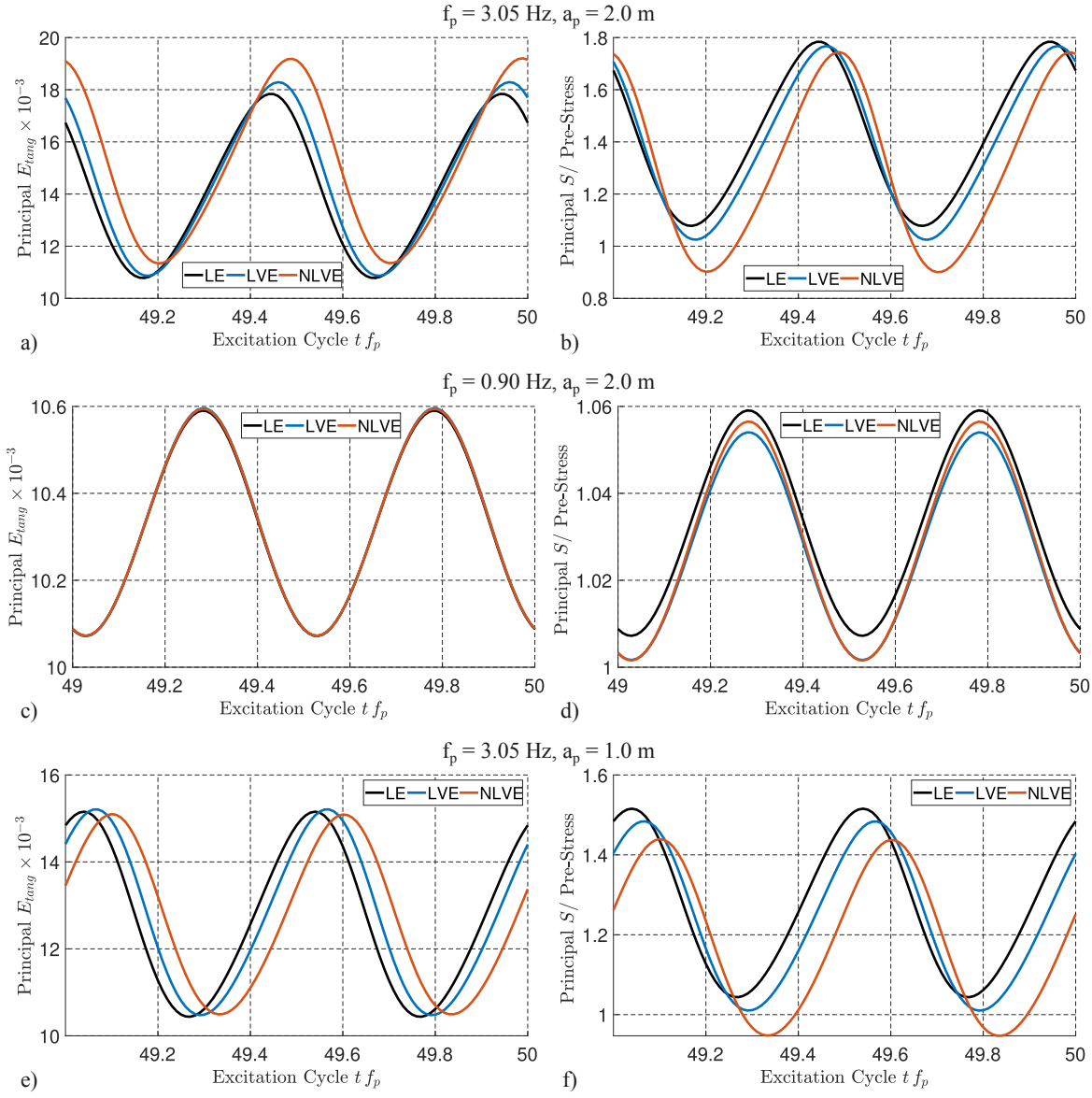

Fig. 9 Plots of principal strain $\mathbf{E}_{\text{tang}}$ and principal stress $\mathbf{S}$ at the fairlead, for taut mooring line subjected to a-b) $f_p = 3.05\,\text{Hz}$ and $a_p = 2.0\,\text{m}$, c-d) $f_p = 0.90\,\text{Hz}$ and $a_p = 2.0\,\text{m}$, e-f) $f_p = 3.05\,\text{Hz}$ and $a_p = 1.0\,\text{m}$. The results are compared across linear-elastic (LE), linear viscoelastic (LVE) and non-linear viscoelastic (NLVE) constitutive relationships.

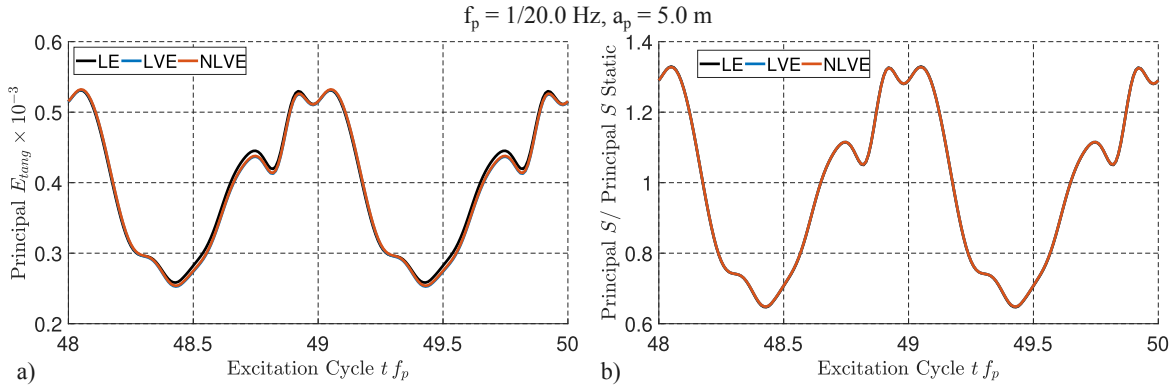

Fig. 10 Plots of principal strain $\mathbf{E}_{\text{tang}}$ and principal stress $\mathbf{S}$ at the fairlead, for catenary line subjected to $f_p = 1/20.0\,\text{Hz}$ and $a_p = 5.0\,\text{m}$. The results are compared across linear-elastic (LE), linear viscoelastic (LVE) and non-linear viscoelastic (NLVE) constitutive relationships.

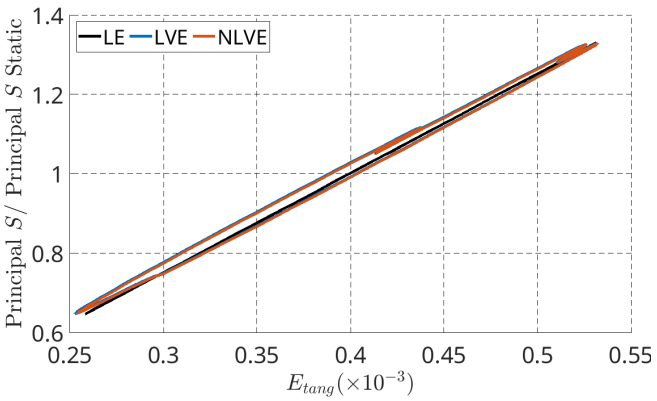

Fig. 11 Plots of principal $\mathbf{E}_{\text{tang}}$ strain against principal $\mathbf{S}$ stress at the fairlead, to indicate the stiffness of the line at the fairlead for the final 25 excitation cycles.

significant role only in high-stress scenarios, which explains the negligible effect of material viscoelasticity in our test case. Synthetic mooring lines are designed to derive their restoring force primarily from material elasticity rather than weight. As a result, they are typically deployed with chain segments near the seabed to introduce tension in the synthetic section and protect it from seabed-induced damage. Building on this model, we plan to investigate multi-segment mooring lines in our future studies.

CONCLUSIONS

This manuscript presents a finite-element model that accounts for the geometric nonlinearity of large displacements and the dynamic non-linear stiffness of synthetic mooring lines. The proposed model is applied to study the dynamic behaviour of a Kapa Polyester Plus synthetic mooring line. The rope was characterized using a non-linear Schapery viscoelastic model, with parameters identified from experimental work by Colomés et al. (2025). Simulations were conducted using three constitutive models: Linear Elastic (LE), Linear Viscoelastic (LVE), and Nonlinear Viscoelastic (NLVE), applied to both taut and catenary mooring configurations.

For taut lines, significant viscoelastic effects were observed under high-frequency, high-amplitude excitation. The NLVE model captured both creep in strain and stress relaxation more accurately than the LVE model, which tended to underestimate non-linear stiffness variation. Phase lags and hysteresis loops in stress-strain responses further highlighted the damping introduced by viscoelasticity. Importantly, non-linear creep was closely linked with geometric nonlinearity, becoming prominent only when both excitation frequency and amplitude were high. Stress relaxation, in contrast, was found to be mainly governed by material viscoelasticity.

In contrast, the catenary configuration showed minimal sensitivity to viscoelastic effects under the tested low-frequency, low-stress condition. The dynamic response was largely governed by the line's geometry and weight-induced restoring forces. Consequently, both linear and nonlinear viscoelastic models produced similar results, with negligible drift or hysteresis. This aligns with the practical design philosophy of using chain segments at the seabed to preload synthetic ropes and enhance their elasticity-driven restoring capacity.

These findings suggest that the conventional industry practice of using a minimum linear stiffness approach for excursion analysis and a maximum linear stiffness approach for load analysis is an oversimplification. This model is thus a step towards developing a tool for understanding synthetic mooring line designs in floating renewable energy systems.

ACKNOWLEDGMENTS

This publication is part of the project MERGANSER with file number DEI122010 of the programme DEI+ from the Netherlands Enterprise Agency (RVO).

REFERENCES

Badia, S. and Verdugo, F. (2020). Gridap: An extensible Finite Element toolbox in Julia. *Journal of Open Source Software*, 5(52):2520.

Banks, H. T., Hu, S., and Kenz, Z. R. (2011). A Brief Review of Elasticity and Viscoelasticity for Solids. *Advances in Applied Mathematics and Mechanics*, 3(1):1–51.

Chung, J. and Hulbert, G. M. (1993). A time integration algorithm for structural dynamics with improved numerical dissipation: The generalized-alpha method. *Journal of Applied Mechanics*, 60(2):371–375.

Colomés, O., Tang, J., Sakthivel, S., Agarwal, S., Jonathan, K., and Gomez, S. (2025). Experimental and Numerical Modeling of Flexible Synthetic Mooring Lines for Floating Structures. In *Proceedings of 35th International Ocean and Polar Engineering Conference*, Seoul, South Korea.

Fries, T. and Schöllhammer, D. (2020). A unified finite strain theory for membranes and ropes. *Computer Methods in Applied Mechanics and Engineering*, 365:113031.

Haj-Ali, R. M. and Muliana, A. H. (2004). Numerical finite element formulation of the Schapery non-linear viscoelastic material model. *International Journal for Numerical Methods in Engineering*, 59(1):25–45.

Hall, M. and Goupee, A. (2015). Validation of a lumped-mass mooring line model with DeepCwind semisubmersible model test data. *Ocean Engineering*, 104:590–603.

Jamshidi, M. and Shokrieh, M. (2024). On the Schapery nonlinear viscoelastic model: A review. *European Journal of Mechanics - A/Solids*, 108:105403.

Lai, J. and Bakker, A. (1996). 3-D schapery representation for nonlinear viscoelasticity and finite element implementation. *Computational Mechanics*, 18(3):182–191.

Nguyen, N. and Thiagarajan, K. (2022). Nonlinear viscoelastic modeling of synthetic mooring lines. *Marine Structures*, 85:103257.

Schapery, R. A. (1969). On the characterization of nonlinear viscoelastic materials. *Polymer Engineering & Science*, 9(4):295–310.

Weller, S., Johanning, L., Davies, P., and Banfield, S. (2015). Synthetic mooring ropes for marine renewable energy applications. *Renewable Energy*, 83:1268–1278.